IEEE Photonics Journal
An IEEE Photonics Society Publication

Open Access

Dual-Channel Light Intensity Modulation Method for Focusing in Projection Lithography

Volume 8, Number 1, February 2016

Yanli Li
Wei Yan
Song Hu
JinHua Feng
Jian Wang

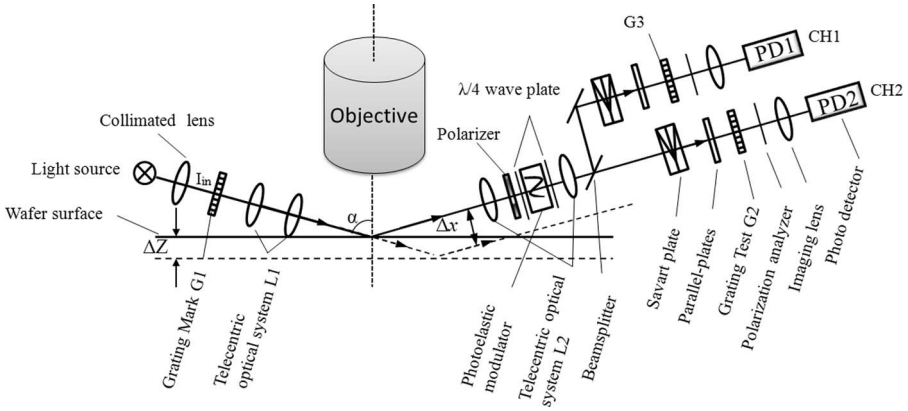

DOI: 10.1109/JPHOT.2015.2508419
1943-0655

IEEE photonics SOCIETY

IEEE

Dual-Channel Light Intensity Modulation Method for Focusing in Projection Lithography

Yanli Li, Wei Yan, Song Hu, JinHua Feng, and Jian Wang

State Key Laboratory of Optical Technologies for Microfabrication, Institute of Optics and Electronics, Chinese Academy of Sciences, Chengdu 610209, China

DOI: 10.1109/JPHOT.2015.2508419

Manuscript received November 17, 2015; revised December 5, 2015; accepted December 9, 2015. Date of current version December 23, 2015. This work was supported by the National Natural Science Foundation of China under Grant 61274108, Grant 61204114, and Grant 61376110. Corresponding author: W. Yan (e-mail: yanwei@ioe.ac.cn).

Abstract: Focusing technique is the key factor in improving the resolution of projection lithography. In order to achieve high accuracy of focusing on the nanometer level, we present a focusing method based on dual-channel light intensity modulation. Two superposed grating fringes are formed with a phase difference of $\pi/2$. The shift of the wafer can be resolved by the phase variation of corresponding fringes. The conventional focusing method with light intensity modulation is influenced by disturbing effects such as fluctuations of the light intensity and stray light. These adverse factors are overcome by the signal ratio of two channels with the same optical components. The focusing accuracy in our experiments is ±8 nm.

Index Terms: Focusing, gratings, lithography, fringe analysis.

1. Introduction

In the last 20 years, optical projection lithography technology experienced 193 nm lithography, immersion lithography, and double patterning and is developing toward Extreme Ultraviolet Lithography (EUV) with wavelength of 13.5 nm. The resolution of lithography is correspondingly improving from 32 nm to 22 nm, and toward the lower 14 nm node [1]–[4]. However, the improvement of resolution is at the expense of decreasing the depth of focus (DOF). The wafer surface fluctuating caused by vacuum adsorption and resist thickness farther shorten the DOF. At present, even though using off-axis lighting wavefront engineering technology, the DOF of the projection lithography equipment is only hundreds of nanometers [3]–[6]. In order to ensure the quality of exposure pattern, a high accuracy measuring scheme for focus detection system is requested.

In the early stage optical, focusing usually employ the slit photometric focusing method [7], [8], which was limited by the serious dependence of slit image quality and image processing algorithm, and the focus accuracy was only hundreds of nanometers and could only apply to the early lower precision lithography. Afterwards, the focusing technique based on laser interference [9], [10], which was characterized by high focusing accuracy, emerged. Nevertheless, the multilayer interference effects between resist films and the fragile environment adaptability seriously

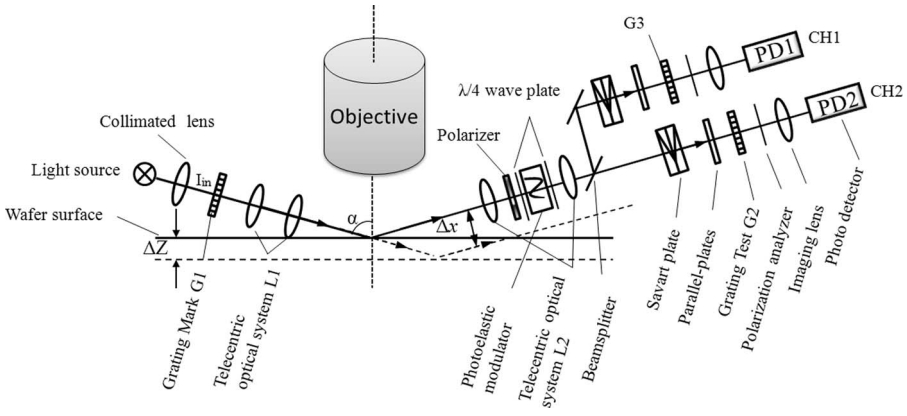

Fig. 1. Diagram of superposed grating dual-channel focusing scheme.

impeded its application as a lithography tool. Recently, moiré fringe technology [11]–[13], which is produced by using two gratings with close periods, was introduced into wafer focusing. Its accuracy at the nanometer level and well technical adaptability make this method be a promising backuép focusing scheme. However, the Talbot effects of grating self-image would cause a decrease in the moiré fringe contrast, as well as some negative impacts on experimental debugging. At present, the main focusing method is still based on light intensity modulation, which is easy to realize and of high precision [14]. However, focusing accuracy can be influenced by the disturbing effects like fluctuations of light intensity, stray light, and so on.

To overcome the adverse factors above mentioned, a focusing method based on dual-channel superposed grating fringe intensity modulation is presented. The method not only inherits the advantage of easy realization and high precision from the conventional method [14] but eliminates the influences from disturbing effects like fluctuations of light intensity and stray light as well. In this paper, we derive the feasibility of the focusing method in theory. Then, we simulate and analyze the influential factors. Finally, the experimental system is set up and the experimental results show that the accuracy of our focusing system is within 8 nm.

2. Principle

This method based on dual-channel superposed grating fringe intensity modulation is shown in Fig. 1. At a large incident angle (α), the Grating Mark (G1) is projected onto the surface of the wafer, reflected, and divided into the first transmitted light and the second transmitted light. Subsequently, the image of G1 is projected onto the Grating Tests (G2 and G3) again, forming the superposed grating with G2 and G3, respectively. The optical paths of CH1 and Ch2 are same. The parallel-plates (P1 and P2) are introduced into the Channel I (CH1) and Channel $\prod$ (CH2) in order to form phase difference of $\pi/2$ between the superposed grating of G1G2 and the superposed grating of G1G3. The photo detectors (PD1 and PD2) measure the amount of light transmitted by the superposed grating G1G2 and G1G3, respectively. Moving the wafer up or down will shift the position of the image of G1 on the G2 and the G3. Consequently, the light intensity on two detectors will change. The focus position of the wafer can be calculated by the ratio of the detector signals.

The telecentric optical systems (L1 and L2) make sure that the image of the G1 is imaged on the Grating Tests. The photoelastic modulator as a high-frequency carrier increases the system performance by resisting interference and noise. The light source illuminates on the G1 with collimated lights (I_{in}). The optical components are analyzed with Jones matrix [15], [16] here. Since the CH1 and the CH2 use the same optical components, we only need to analyze CH1. CH2 can be deduced by CH1. In CH1, the I_{PD1} is sheared into two beams by SAVART plate, namely,

ordinary light $(I_o(\Delta x))$ and extraordinary light $(I_e(\Delta x))$ with mutual orthogonality. The light intensity after the G3 is expressed as [17], [18]

$$\begin{cases} I_o(\Delta x) = \frac{kI_{in}}{2}\left(\frac{1}{4} + \frac{2}{\pi^2}\cos\left(\frac{2\pi(\Delta x - s)}{p}\right)\right)(1 + \sin\delta(t)) \\ I_e(\Delta x) = \frac{kI_{in}}{2}\left(\frac{1}{4} + \frac{2}{\pi^2}\cos\left(\frac{2\pi(\Delta x + s)}{p}\right)\right)(1 - \sin\delta(t)). \end{cases} \tag{1}$$

$k \in [0, 1]$ is the beam splitter reflectivity, Δx is the shift position of the image of G1, 2 s is the shearing of Savart plate, p is the period of the gratings, and $\delta(t) = \pi\sin(2\pi\ \mathrm{ft})/2$, which is the phase difference between photoelastic modulator and the incidence light beam.

Because the detector cannot distinguish the polarization of beams, the received energy is the sum from all received beams. The light intensity detected by the PD1 is expressed as

$$\begin{aligned} I_{PD1} &= I_o(\Delta x) + I_e(\Delta x) \\ &= \frac{kI_{in}}{2}\left(\frac{1}{2} + \frac{4}{\pi^2}\cos\frac{2\pi\Delta x}{p}\cos\frac{2\pi s}{p}\right) + \frac{kI_{in}}{2}\left(-\frac{4}{\pi^2}\sin\frac{2\pi\Delta x}{p}\sin\frac{2\pi s}{p}\right) \times \sin\delta(t). \end{aligned} \tag{2}$$

Based on (2), there are two terms containing the shearing s, but only the second term is affected by photoelastic modulator. Obviously, the detected light intensity has the best signal noise ratio, when the first term cos $(2\pi s/p)$ is 0. Therefore, when the $s = p/4$, (2) can be expressed as

$$I_{PD1} = \frac{kI_{in}}{4} + \frac{2kI_{in}}{\pi^2}\sin\frac{2\pi\Delta x}{p}\sin\delta(t). \tag{3}$$

Without regard to direct current, the signal of the PD1 is rewritten as

$$I_{PD1} = \frac{2kI_{in}}{\pi^2}\sin\frac{2\pi\Delta x}{p}\sin\delta(t). \tag{4}$$

The phase difference between CH2 and CH1 is $\pi/2$ formed by the parallel-plates. Therefore, the signal of the PD2 is expressed as

$$I_{PD2} = \frac{2(1-k)I_{in}}{\pi^2}\sin\left(\frac{2\pi\Delta x}{p} + \frac{\pi}{2}\right)\sin\delta(t). \tag{5}$$

If the transmitted light energy is equally divided by the beam splitter, that is, $k = 0.5$, according to (4) and (5), the shift (Δx) of image of G1 is

$$\Delta x = \frac{p}{2\pi}\arctan\left(\frac{I_{PD1}}{I_{PD2}}\right). \tag{6}$$

Based on the grazing incident beam method, the Δx is induced by the vertical move (ΔZ) of the wafer in this scheme. $\Delta x = \Delta Z \cdot \sin 2\alpha/\cos\alpha = 2\Delta Z \cdot \sin\alpha$ as shown in Fig. 1, where α is the incident angle with respect to the surface of the wafer. As a result, the change in the height of the wafer is expressed as

$$\Delta Z = \frac{p}{4\pi\sin\alpha}\arctan\left(\frac{I_{PD1}}{I_{PD2}}\right). \tag{7}$$

The shift height of wafer can be calculated by solving arc tangent of the signals detected by two detectors. This scheme changes one channel into two received channels with the same optical components and introduces the adjustable parallel-plates forming the phase difference of $\pi/2$, which effectively eliminates the fluctuations of the light intensity by the ratio I_{PD1}/I_{PD2}.

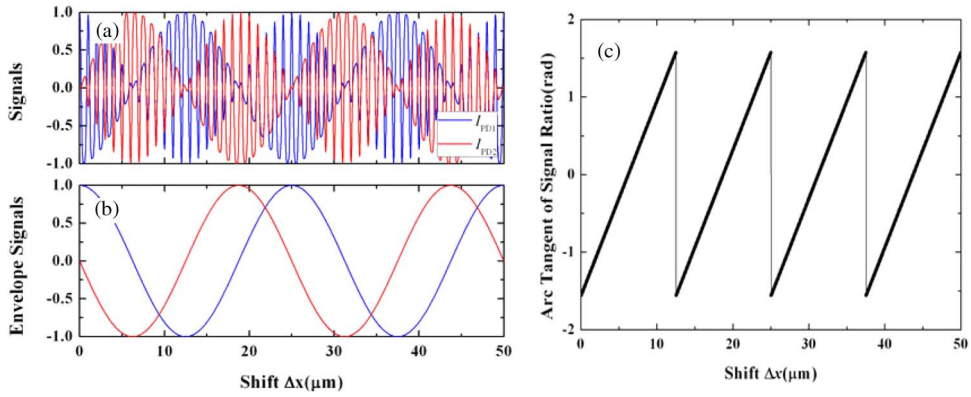

Fig. 2. (a). Signals of the two detectors with the shift in 0.05 μm step. (b) Corresponding envelope waveform of Fig. 2(a). (c) Arc tangent of signal ratio between the PD1 and the PD2.

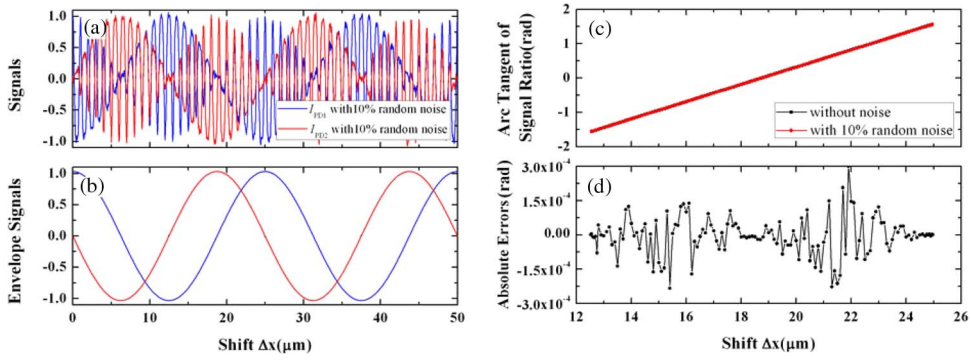

Fig. 3. (a) Signals of two detectors with 10% random noise. (b) Corresponding envelope waveform of Fig. 3(a). (c) Arc tangent of signal ratio between the PD1 and the PD2 in one grating period. (d) Absolute errors between arc tangent of signal ratio without noise and arc tangent of signal ratio with noise.

3. Simulation

To confirm the validity of this scheme, we simulated the signals of two detectors with the Δx increasing at a constant amount. The signals do not include the output direct current signal. The simulated results and the corresponding envelope signals of PD1 and PD2 are shown in Fig. 2(a) and (b), respectively. The period of grating p is 25 μm. The phase difference is $\pi/2$. Therefore, the changing of two signals takes on sine curve and cosine curve with the Δx increasing, respectively. The arc tangent of signal ratio between the two detectors is shown in Fig. 2(c). The curve periodically changes with the Δx increasing, and the period is 12.5 μm ($p/2$); the influence factors within one period is typical. Without considering the influence of other factors such as environmental temperature, the shift in height of the wafer can be obtained from the ratio between the signal of PD1 and the signal of PD2. Therefore, the accuracy of the arc tangent of the signal ratio directly determines the accuracy of the focusing system.

3.1. The Influences of Random Noise

Fig. 3(a) is the signal with 10% random noise with the shift x in steps of 0.05 μm. The 10% random noise is defined as the ratio of 10% between maximal amplitude of random noise and the maximal amplitude of the signal (I_{PD1} or I_{PD2}). The I_{PD1} and I_{PD2} take noise of uniform distribution independently. Fig. 3(b) is the corresponding envelope signal of Fig. 3(a). The smooth envelope curve is obtained by a band-pass filter. The mathematical form is rect $((f - f_0)/w)$, where f is the frequency of filter, f_0 is the center of filter, and w is the bandwidth. The arc

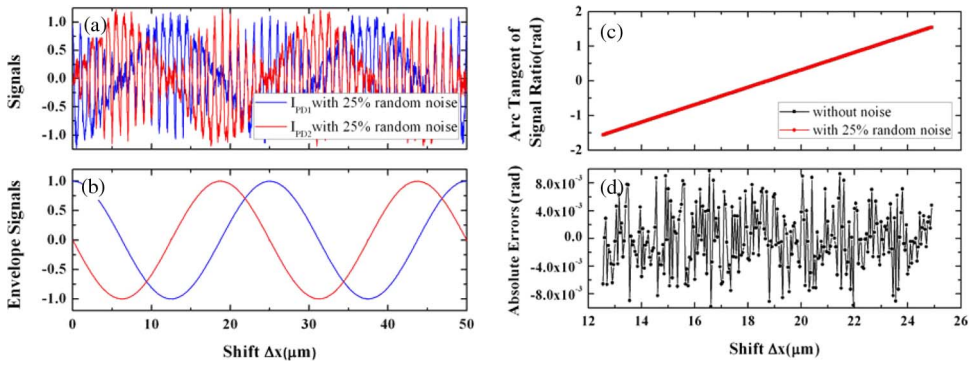

Fig. 4. (a) Signals of two detectors with 25% random noise. (b) Corresponding envelope waveform of Fig. 4(a). (c) Arc tangent of signal ratio between the PD1 and the PD2 in one grating period. (d) Absolute errors between arc tangent of signal ratio without noise and arc tangent of signal ratio with noise.

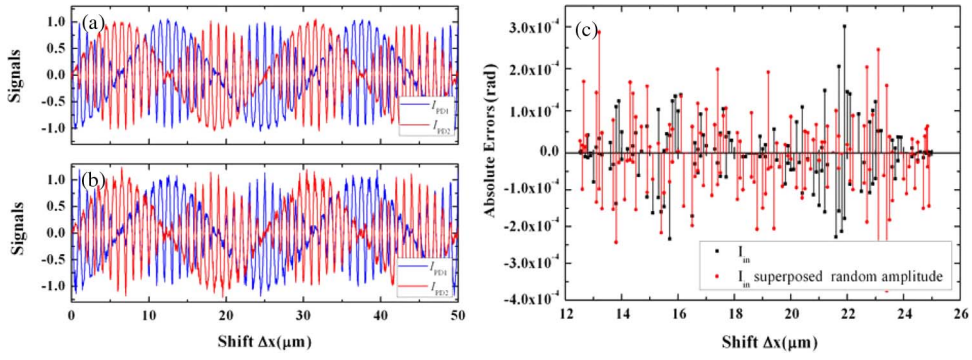

Fig. 5. (a) Signals of the two detectors with the constant light intensity. (b) Signals of the two detectors with the fluctuating light intensity. (c) Absolute errors with the constant light intensity and the fluctuating light intensity.

tangents of signal ratio without noise and with noise are shown in Fig. 3(c). The simulation shows that the red curve and the black curve almost overlap together. The arc tangent of signal ratio is linear affected by the Δx. As a result, an inconspicuous change in the arc tangent of signal ratio is correlated with a distinct vertical move of the wafer. The absolute errors between arc tangent of signal ratio without noise and arc tangent of signal ratio with noise are shown in Fig. 3(d). The absolute errors fluctuation within 3.0×10^{-4} rad in one period range between 12.5 and 25 μm and the RMS error is 8.86×10^{-5} rad.

The RMS errors with random noise of 15%, 20%, and 25%, are 8.8×10^{-4} rad, 3.2×10^{-3} rad and 5.4×10^{-3} rad, respectively. The absolute error increases with the increase of the ratio of random noise. Fig. 4(a) is the signal with 25% random noise with the shift x in 0.05 μm step. The absolute errors between arc tangent of signal ratio without noise and arc tangent of signal ratio with noise are shown in Fig. 4(d). According to (7), the RMS error caused by random noise of the focusing system will exceed 10 nm until the signal with 25% random noise. The simulation results prove that the focusing method has a very good ability to resist noise.

3.2. The Influences of Light Intensity Fluctuations

The fluctuation of light intensity caused by the fluctuations of the light source or reflectance of the wafer surface is the major error source for focusing system. We simulate the intensity fluctuations by superposition the random amplitude with variance of 0.1 and the I_{in}, and compare the absolute errors with the I_{in}. The signals with 10% random noise are shown in Fig. 5(a) and (b),

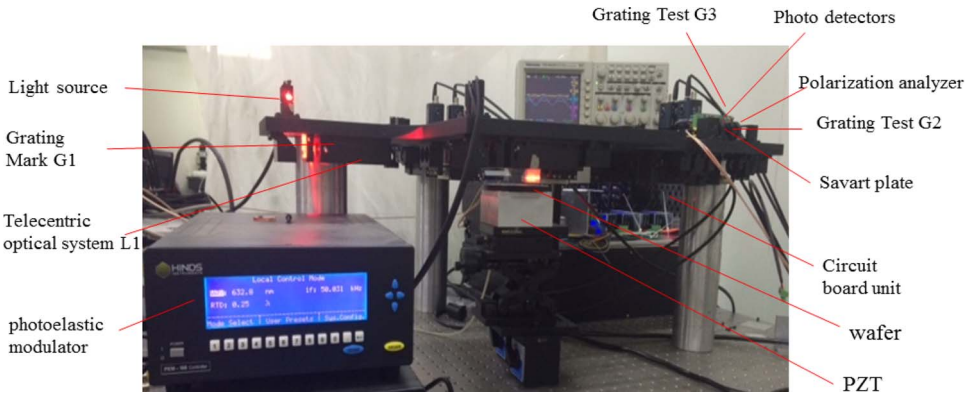

Fig. 6. Experimental setup conducted according to the schematic in Fig. 1.

respectively, when the light intensity is the I_{in} and the I_{in} superposed random amplitude. The Absolute errors transform with the Δx are shown in Fig. 5(c).

The absolute errors with different intensities fluctuate within 3.4×10^{-4} rad ranges between 12.5 μm and 25 μm. The RMS error with the constant light intensity and the fluctuating light intensity are 8.86×10^{-5} rad and 9.06×10^{-5} rad, respectively. The results show that the influence of the light intensity fluctuations is eliminated. The important source of absolute errors is the random noise. That is, this focusing method has strong anti-jamming capability and high precision.

4. Experimental Results and Discussions

In order to verify our analysis mentioned above, an experimental system for the focusing scheme is set up as illustrated in Fig. 6. The incident light is generated by collimating the LED illumination source with main wavelength 530 nm, spectral bandwidth 30 nm and optical power 0.86 mW. The photoresist-coated wafer is fixed on a piezoelectric translator (PZT, the resolution, and stroke are 2 nm (closed loop) and 150 μm, respectively).

The PZT is used for the defocusing control. The G1 is projected onto the surface of wafer at the incident angle 86°, and is reflected and modulated by the photoelastic modulator (HINDS) with the wavelength 632 nm and the modulation frequency 50 kHz. Then, the transmitted light is divided into two beams. The image of G1 with G2 and G3 forms the superposed gratings. The thickness of Savart plate is 6.06 mm. The PD1 and PD2 measure the amount of light transmitted by the superposed grating. The periods of G1, G2, and G3 are both 25 μm and the lenses L1 and L2 have the same magnification (×1). The system's NA is 0.02. The phase difference formed by the P1 and P2 is 88°. The voltage values of CH1 and CH2 are shown in Fig. 7(a), where the PZT produces wafer displacement from 3 μm to 40 μm in 0.05 μm steps. In addition, the experiment with fluctuations of light intensity is carried out by attenuating the light source to 80%. The results are shown in Fig. 7(b).

When the PZT produces wafer displacement from 10 μm to 20 μm in 0.1 μm steps, the absolute errors between the focusing results and PZT displacement are shown in Fig. 8. The maximal errors, the mean absolute errors and the RMS errors with the light source unattenuated and the light source attenuated to 80% are 7.89 nm, 2.1 nm, 2.83 nm, 7.93 nm, 2.48 nm, and 3.11 nm, respectively. The negligible errors may be from environmental disturbance, algorithm error and PZT step error. The results show that the small amount of attenuation on the light intensity does not influence the measured height.

5. Conclusion

The focusing method based on dual-channel superposed grating fringe intensity modulation for projection lithography is presented. The shift height of the wafer is calculated by solving the arc

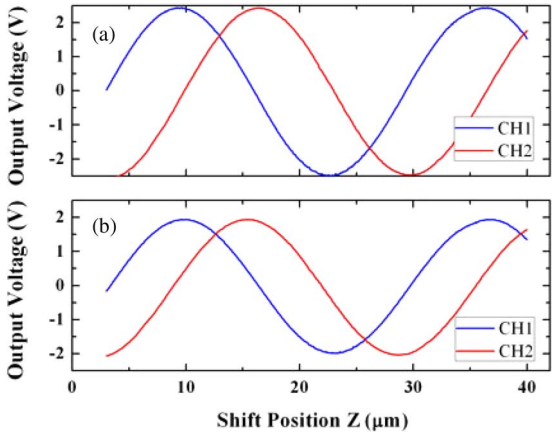

Fig. 7. (a) Experimental results with the light source unattenuated. (b) Experimental results with the light source attenuated to 80%.

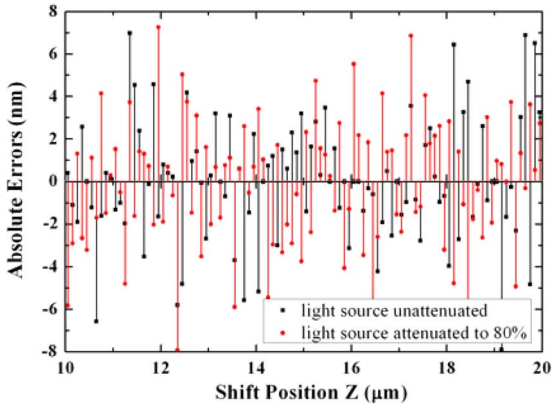

Fig. 8. Absolute errors between focusing results and PZT displacement.

tangent of the signal ratio of the two detectors, and the major error sources such as fluctuations of the light intensity and stray light, which affect the accuracy of the focusing system, are eliminated. This method is verified with via simulation and experiment, and strong anti-jamming capability and accuracy of the nanometer level are achieved. This new method is suitable to be used in high-precision project lithography.

References

[1] K. Ronse *et al.,* "Lithography options for the 32 nm half pitch node and beyond," in *Proc. IEEE Custom Integr. Circuits Conf.*, 2008, pp. 371–378.
[2] S. Owa, S. Wakamoto, M. Murayama, H. Yaegashi, and K. Oyama, "Immersion lithography extension to sub-10 nm nodes with multiple patterning," in *Proc. SPIE, Opt. Microlithogr.*, Feb. 2014, vol. 9052, pp. 1–9.
[3] K. Tawarayama *et al.,* "Recent progress of EUV full-field exposure tool in Selete," in *Proc. SPIE, Adv. Lithogr.*, Mar. 2009, vol. 727, pp. 118–125.
[4] J. H. Jang *et al.,* "Focus control budget analysis for critical layers of flash devices," in *Proc. SPIE*, 2014, vol. 9050, pp. 1–7.
[5] F. Kahlenberg *et al.,* "Best focus determination: Bridging the gap between optical and physical topography," in *Proc. Adv. Lithogr., Int. Soc. Opt. Photon.*, Mar. 2007, vol. 6520, pp. 1–8.
[6] T. Huang, S. Liu, P. Yi, and T. Shi, "Focusing and leveling system for optical lithography using linear CCD," in *Proc. Int. Conf. Opt. Instrum. Technol.*, Dec. 2008, vol. 7160, pp. 1–6.

[7] J. E. van der Werf, "Optical focus and level sensor for wafer steppers," *J. Vac. Sci. Technol. B*, vol. 10, no. 2, pp. 735–740, Mar. 1992.
[8] Y. Oshida, "Chip leveling and focusing with laser interferometry," in *Proc. SPIE*, 1990, vol. 1264, pp. 244–251.
[9] M. Watanabe, "Focusing and leveling based on wafer surface profile detection with interferometry," in *Proc. SPIE*, 1994, vol. 2197, pp. 809–989.
[10] W. Yan, Y. Yang, W. Chen, S. Hu, and S. Zhou, "Moiré based focusing and leveling scheme for optical projection lithography," *Appl. Opt.*, vol. 49, no. 31, pp. 5959–5963, May 2010.
[11] S. Zhou *et al.,* "Fourier-based analysis of moiré fringe patterns of superposed gratings in alignment of nanolithography," *Opt. Exp.* vol. 16, no. 11, pp. 7869–7880, 2008.
[12] C. Di *et al.,* "Interferometric scheme for high-sensitivity coaxial focusing in projection lithography," *IEEE Photon. J.*, vol. 6, no. 3, pp. 167–174, Jun. 2014.
[13] N. Gao and C. Xie, "High-order diffraction suppression using modulated groove position gratings," *Opt. Lett.*, vol. 36, no. 21, pp. 4251–4253, Nov. 2011.
[14] A. J. Zeng, X. C. Wang, and D. Y. Xu, "Progress in focus and level sensor for projection lithography," *Laser Optoelectron. Progress*, vol. 41, no. 7, pp. 24–30, Apr. 2004.
[15] M. Gaugitsch and H. Hauser, "Optimization of a magneto-optical light modulator—Part I: Modeling of birefringence and Faraday effect," *J. Lightw. Technol.* vol. 17, no. 12, pp. 2633–2644, 1999.
[16] A. J. Zeng and X. Z. Wang, "Application of photoelastic modulator in modulation of polarization direction," *Chin. J. Lasers*, vol. 32, no. 8, pp. 1063–1067, Aug. 2005.
[17] C. Di, W. Yan, and S. Hu, "Technology of focus detection for 193 nm projection lithographic tool," in *Proc. SPIE, Int. Symp. Adv. Opt. Manuf. Test. Technol., Des., Manuf., Test. Smart Struct., Micro-Nano-Opt. Devices, Syst.*, 2012, vol. 8418, pp. 1–9.
[18] X. Li, F. Chen, and Z. Li, "Simulation on signal processing of focusing and leveling measurement system," in *Proc. SPIE, Int. Symp. Adv. Opt. Manuf. Test. Technol., Des., Manuf., Test. Smart Struct., Micro-Nano-Opt. Devices, Syst.*, 2007, vol. 6724, pp. 1–9.